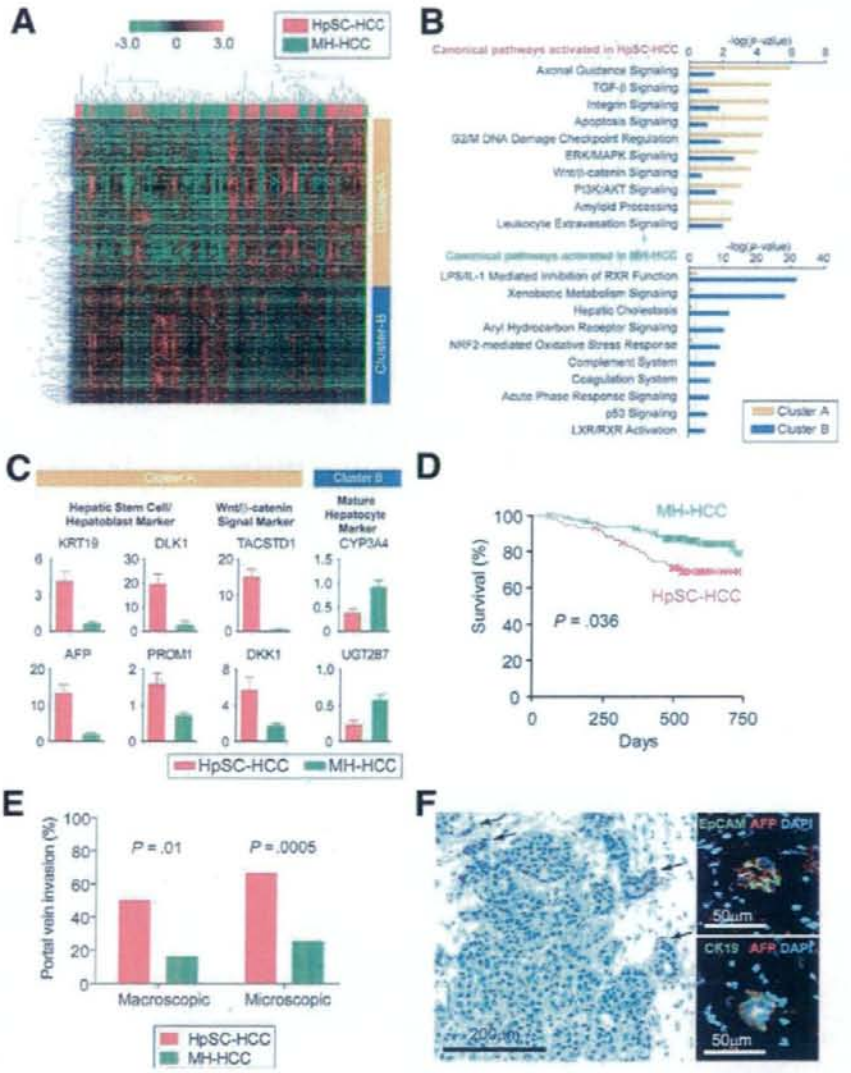

Figure 1. HpSC–HCC represents a subset of invasive HCCs with CSC features. (A) Hierarchical cluster analysis based on 793 HpSC–HCC–coregulated genes in 156 HCC cases. Each cell in the matrix represents the expression level of a gene in an individual sample. Red and green cells depict high and low expression levels, respectively, as indicated by the scale bar. (B) Pathway analysis of HpSC–HCC–coregulated genes. The top 10 canonical signaling pathways activated in cluster A (upper panel) or cluster B (lower panel) with statistical significance ($P < .01$) are shown. (C) Expression patterns of well-known HpSC and MH markers in each HCC subtype as analyzed by microarray. (D) Kaplan–Meier survival analysis of the cases used for array analysis. (E) Frequency of macroscopic and microscopic portal vein invasion in HpSC-HCC and MH-HCC used for IHC. (F) Representative images of EpCAM, AFP, and CK19 staining in HpSC–HCC samples analyzed by IHC and IF. EpCAM staining illustrates heterogeneous expression of EpCAM in HpSC-HCC (left panel). EpCAM$^+$ cells were disseminated in the invasive border (left panel black arrows) with expression of AFP (right top panel) and CK19 (right bottom panel).

EpCAM$^+$ and CD133$^+$, but no CD90$^+$ cells, whereas AFP$^-$ cell lines had a subpopulation of CD90$^+$ cells but no EpCAM$^+$ or CD133$^+$ cells (Figure 2*B*). These data indicate that HpSC-HCC and MH-HCC cell lines have distinct stem cell marker expression patterns, and EpCAM as well as CD133 may be hepatic CSC markers specifically in HpSC-HCC.

We selected 2 human HCC cell lines (HuH1 and HuH7) to isolate EpCAM$^+$ cells because both lines were heterogeneous in EpCAM, AFP, CK19, and β-catenin expression (Figure 2*A* and *B* and Supplementary Figure 1*A*; see supplementary material online at www.gastrojournal.org).[29] We successfully enriched EpCAM$^+$ and EpCAM$^-$ populations from HuH7 cells by FACS, with more than 80% purity in EpCAM$^+$ cells and more than 90% purity in EpCAM$^-$ cells 1 day after sorting (Figure 3*A*). Similar results were obtained when the purity check was performed immediately after sorting (data not shown). EpCAM$^+$ cells also were positive for CK19 and β-catenin (Figure 3*B* and Supplementary Figure 1*B*; see supplementary material online at www.gastrojournal.org) and most were AFP$^+$ (data not shown). In contrast, EpCAM$^-$ cells were negative for these markers but positive for HepPar1, a monoclonal antibody specific to hepatocytes (Figure 3*B*). Consistent with the microarray data described earlier, the levels of *TACSTD1*, *MYC*, and *hTERT* (known HpSC markers) were increased significantly in EpCAM$^+$ HuH7 cells, whereas the levels of *UGT2B7* and *CYP3A4*

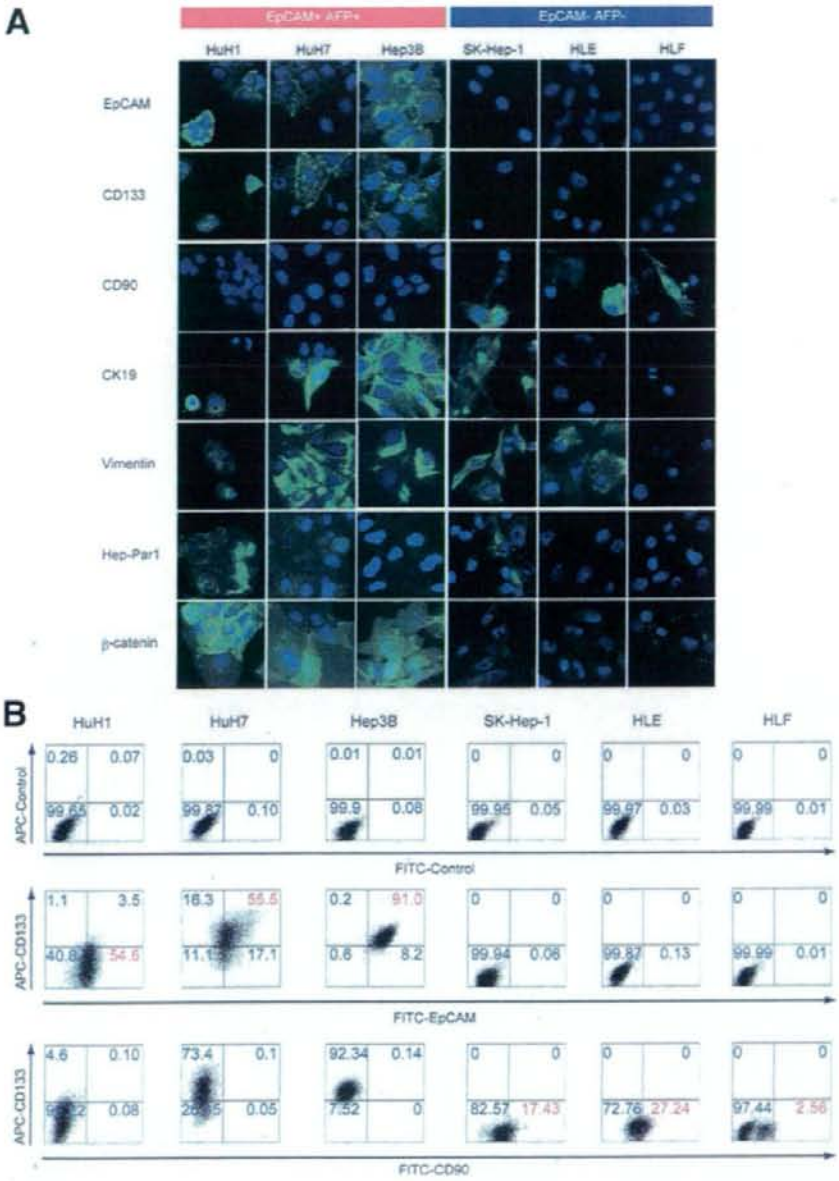

Figure 2. Characterization of hepatic stem cell marker expression in HCC cell lines. (A) IF analysis of 6 HCC cell lines (EpCAM$^+$ AFP$^+$ cell lines: HuH1, HuH7, and Hep3B; EpCAM$^-$ AFP$^-$ cell lines: SK-Hep-1, HLE, and HLF) stained with anti-EpCAM, anti-CD133, anti-CD90, anti-CK19, anti-Vimentin, anti-Hep-Par1, and anti-β-catenin antibodies. (B) FACS analysis of 6 HCC cell lines stained with anti-EpCAM, anti-CD133, and anti-CD90 antibodies.

(known mature hepatocyte markers) were significantly higher in EpCAM$^-$ HuH7 cells (Figure 3C, *left upper panel*). This expression pattern was reminiscent of human HpSC cells (Figure 3C, *left lower panel*). Similar results were obtained from HuH1 cells (data not shown). We also compared gene expression patterns of isolated HuH1, HuH7, MH, and HpSC cells using the TaqMan Human Stem Cell Pluripotency Array (Applied Biosystems, Foster City, CA) containing 96 selected human stem cell-related genes. Although a differential expression pattern of stem cell-related genes was evident among HpSC, EpCAM$^+$ HuH1, and EpCAM$^+$ HuH7 cells, the EpCAM$^+$ HCC cells were related more closely to HpSC cells whereas EpCAM$^-$ HCC cells were related more closely to diploid adult mature hepatocytes (Figure 3C, *right panel*; and Supplementary Figure 1C; see supplementary material online at www.gastrojournal.org). Thus, it appeared that EpCAM$^+$ HCC cells had a gene expression pattern that is related more closely to HpSC than EpCAM$^-$ HCC cells.

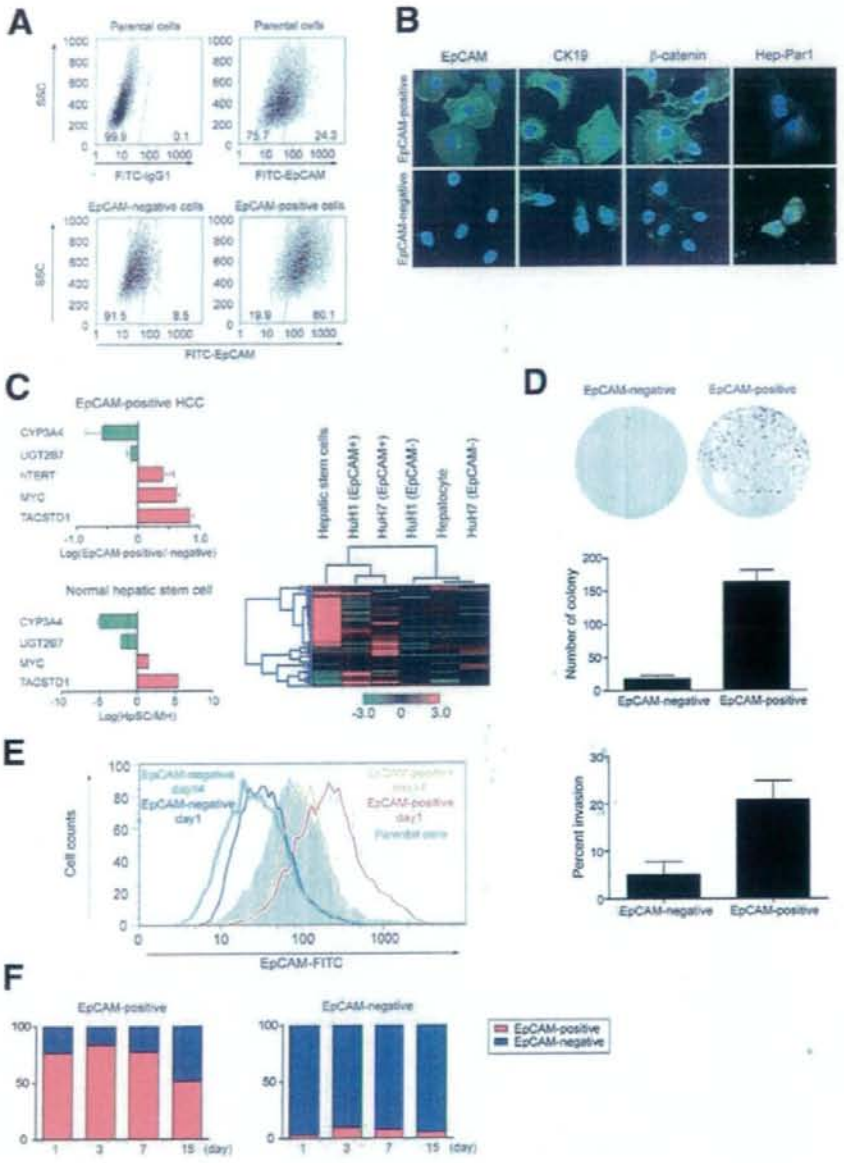

Figure 3. Characterization of EpCAM$^+$ and EpCAM$^-$ cells in HuH7 cells. (A) FACS analysis of EpCAM$^+$ and EpCAM$^-$ cells on day 1 after cell sorting. (B) IF analysis of cells stained with anti-EpCAM, anti-AFP, anti-CK19, or anti–β-catenin antibodies. (C) Quantitative reverse-transcription polymerase chain reaction analysis of EpCAM$^+$ and EpCAM$^-$ HuH7 cells (left upper panel) or HpSCs and MHs (left lower panel). Experiments were performed in triplicate. Hierarchical cluster analysis of HpSC, MH, and EpCAM$^+$ and EpCAM$^-$ HCC cells using a panel of genes expressed in human embryonic stem cells (right panel). Gene expression was measured in quadruplicate. (D) Representative photographs of the plates containing colonies derived from 2000 EpCAM$^+$ or EpCAM$^-$ HuH7 cells (upper panel). Colony formation experiments were performed in triplicate (mean ± SD) (middle panel). Cell invasiveness of EpCAM$^+$ and EpCAM$^-$ cells using the Matrigel invasion assay (lower panel). (E) Flow cytometer analysis of EpCAM$^+$ and EpCAM$^-$ HuH7 cells stained with anti-EpCAM at days 1 and 14 after cell sorting. (F) Percentage of sorted EpCAM$^+$ and EpCAM$^-$ cells after culturing for various times as analyzed by IF. Numbers of EpCAM$^+$ and EpCAM$^-$ cells were counted in 3 independent areas of chamber slides at days 1, 3, 7, and 15 after cell sorting. The average percentages of EpCAM$^+$ or EpCAM$^-$ cells are depicted as red or blue, respectively.

The isolated EpCAM$^+$ HuH7 cells formed colonies efficiently whereas EpCAM$^-$ cells failed to do so (Figure 3*D*, *upper* and *middle panels*; and Supplementary Figure 2*A* for HuH1 cells; see supplementary material online at www.gastrojournal.org). In addition, EpCAM$^+$ HuH7 cells were much more invasive than EpCAM$^-$ cells ($P < .03$) (Figure 3*D*, *lower panel*; and Supplementary Figure 2*B* for HuH1 cells; see supplementary material online at www.gastrojournal.org). The EpCAM$^+$ fraction decreased with time in sorted EpCAM$^+$ HuH7 cells from greater than 80% to 50% (Figure 3*E*). However, a small percentage of EpCAM$^+$ cells remained constant in sorted EpCAM$^-$ HuH7 cells. FACS analysis confirmed the results of IF analysis (Figure 3*F* and Supplementary Figure 2*C* for HuH7 and HuH1 cells, respectively; see supplementary material online at www.gastrojournal.org), suggesting that EpCAM$^+$ cells could differentiate into EpCAM$^-$ cells, eventually allowing an enriched EpCAM$^+$ fraction to revert back to parental cells after 14 days of culture. In contrast, EpCAM$^-$ cells maintained their EpCAM$^-$ status. In addition, we successfully isolated 12 HuH1 and 2 HuH7 colonies from 192 single-cell-plated culture wells.

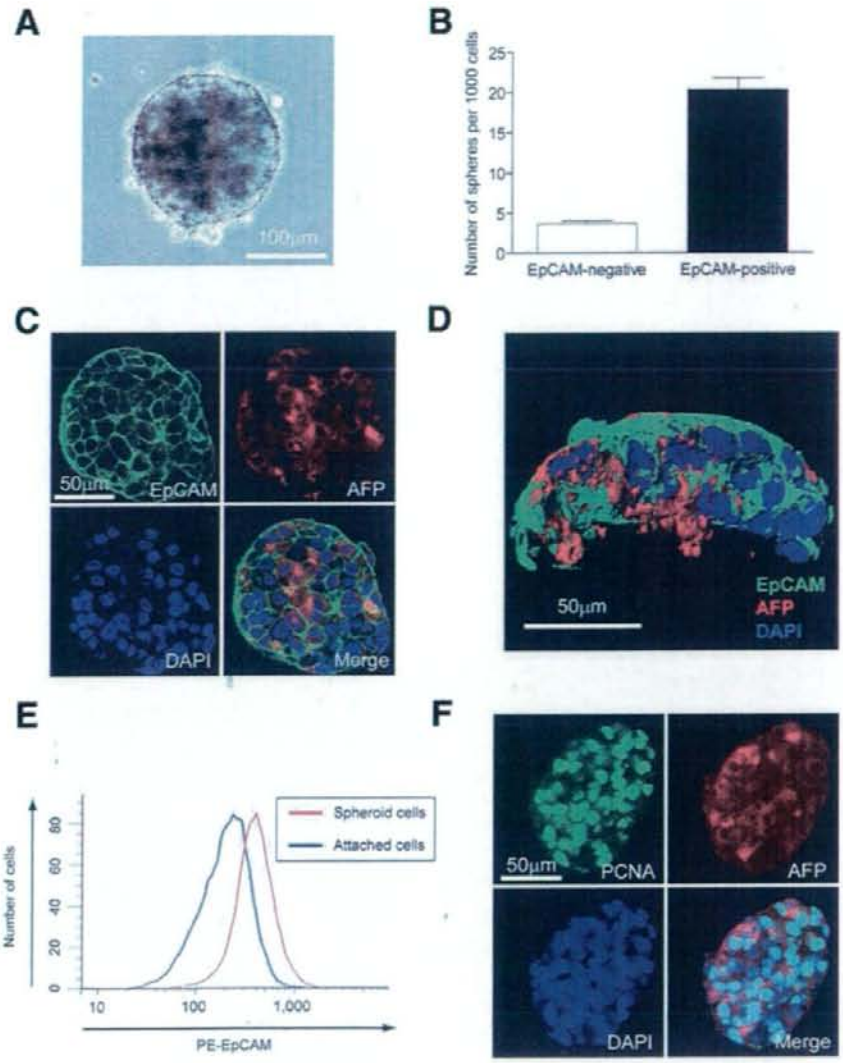

Figure 4. Spheroid formation of EpCAM$^+$ HuH1 HCC cells. (A) A representative phase-contrast image of an HCC spheroid derived from an EpCAM$^+$ cell (scale bar, 100 μm) and (B) total numbers of spheroids from 1000 sorted cells are shown. Experiments were performed in triplicate and data are shown as mean ± SD. (C) Representative confocal images of an HCC spheroid co-stained with anti-EpCAM, anti-AFP, and 4′,6-diamidino-2-phenylindole (DAPI) (scale bar, 50 μm). (D) A 3-dimensional image of an HCC spheroid co-stained with anti-EpCAM, anti-AFP, and DAPI (scale bar, 50 μm) reconstructed from confocal images using surface rendering. (E) FACS analysis of EpCAM$^+$ cells cultured as spheroid cells (red) or attached cells (blue) for 14 days after cell sorting. (F) Confocal images of an HCC spheroid co-stained with anti-PCNA, anti-AFP, and DAPI (scale bar, 50 μm).

However, all colonies were heterogeneous in EpCAM and AFP expression and no colony was completely EpCAM$^-$ (data not shown). Taken together, these results indicate that EpCAM$^+$ HCC cells resemble HpSC features. It appears that EpCAM$^+$ cells, but not EpCAM$^-$ cells, have self-renewal and differentiation capabilities with the ability to form colonies from a single cell, and produce both EpCAM$^+$ and EpCAM$^-$ cells.

It has been shown previously that stem/progenitor cells and cancer stem/progenitor cells can form spheroids in vitro in a nonattached condition.[36,37] Consistently, EpCAM$^+$ cells could form spheroids efficiently, reaching to about 150 to approximately 200 μm in diameter after 14 days of culture (Figure 4*A* and *B*). Interestingly, all cells in a spheroid were EpCAM$^+$, whereas AFP expression was relatively heterogeneous (Figure 4*C* and *D*, and Supplementary movie 1; see supplementary material online at www.gastrojournal.org). Rarely, a few spheroids derived from an EpCAM$^-$ cell fraction were positive for EpCAM (data not shown), suggesting that these spheroids were derived from contaminated residual EpCAM$^+$ cells by FACS sorting. All spheroid cells maintained EpCAM expression while half of the attached cells lost EpCAM expression when the EpCAM$^+$ fraction was cultured for 14 days (Figure 4*E*). Most spheroid cells also abundantly expressed proliferating cell nuclear antigen (PCNA), implying active cell proliferation (Figure 4*F* and Supplementary movie 2; see supplementary material online at www.gastrojournal.org). Thus, a subset of EpCAM$^+$ cells, but not EpCAM$^-$ cells, can form spheroids.

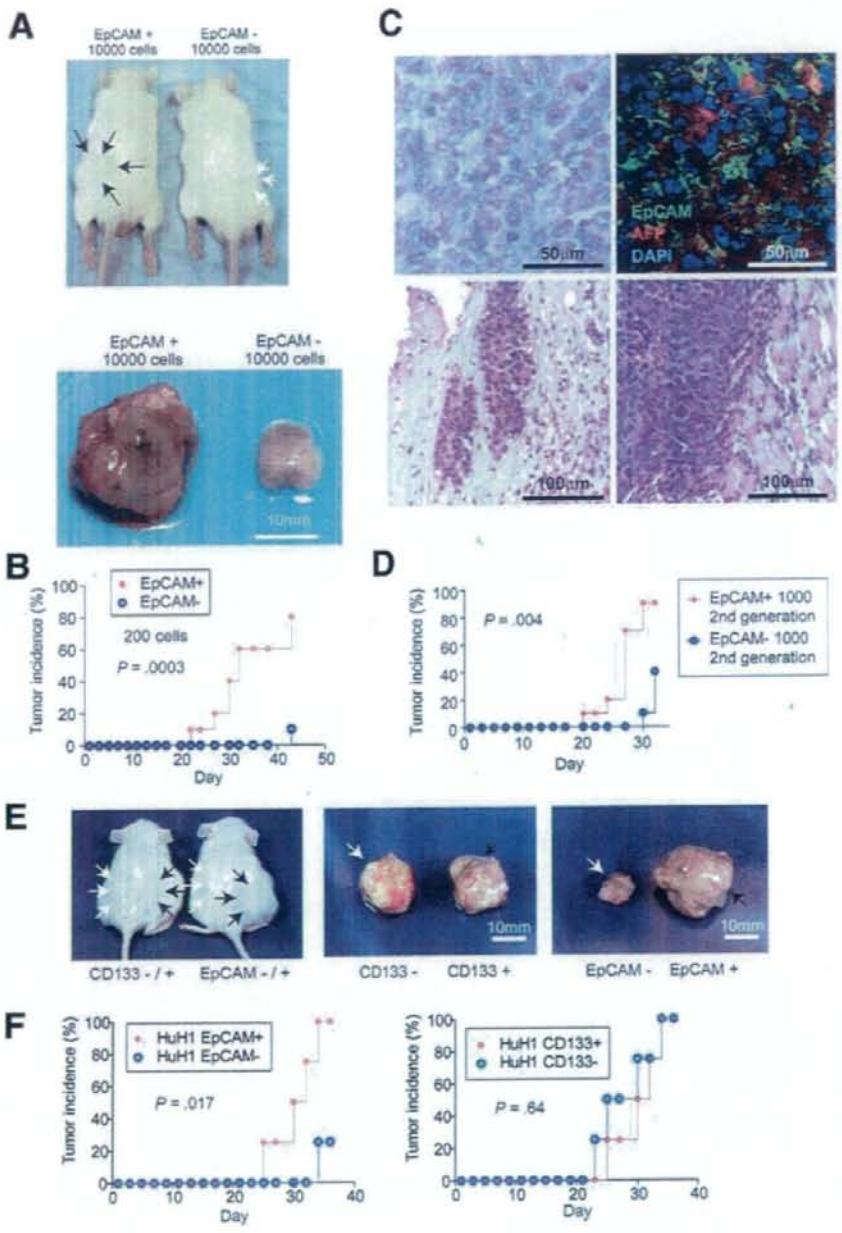

Figure 5. Tumorigenic and invasive potential of EpCAM⁺ HCC cells. (A) Representative NOD/SCID mice (upper panel) with subcutaneous tumors (lower panel) from EpCAM⁺ (black arrows) or EpCAM⁻ (white arrows) HuH1 cells. (B) Tumorigenicity of 200 sorted HuH1 cells. (C) Histologic analysis of EpCAM⁺ HuH1-derived xenografts. H&E staining of a subcutaneous tumor (left upper panel) with capsular invasion (left lower panel) and muscular invasion (right lower panel) and IF of the tumor stained with anti-EpCAM, anti-AFP, and 4′,6-diamidino-2-phenylindole (DAPI) (right upper panel) (scale bar, 50 μm). (D) Tumorigenicity of 1000 sorted cells derived from an EpCAM⁺ HuH1 xenograft. Data are generated from 10 mice in each group. (E) Representative NOD/SCID mice (left panel) with subcutaneous tumors from CD133⁺ (black arrows) or CD133⁻ (white arrows) (middle panel) and EpCAM⁺ (black arrows) or EpCAM⁻ (white arrows) (right panel) HuH1 cells. (F) Tumorigenicity of 1000 HuH1 cells sorted by anti-EpCAM (left panel) or anti-CD133 (right panel) antibodies.

EpCAM⁺ HCC Cells as Tumor-Initiating Cells

EpCAM⁺ HCC cells, but not EpCAM⁻ HCC cells, could efficiently initiate invasive tumors in NOD/SCID mice (Figure 5). For example, 10,000 EpCAM⁺ HuH1 cells produced large hypervascular tumors in 100% of mice whereas EpCAM⁻ cell fractions produced only small and pale-looking tumors in 30% of mice 4 weeks after injection (Figure 5*A* and Supplementary Figure 3*A*; see supplementary material online at www.gastrojournal.org). Similar results were obtained with HuH7 cells (Supplementary Figure 3*B–D*; see supplementary material online at www.gastrojournal.org). As little as 200 EpCAM⁺ cells could initiate tumors in 8 of 10 injected mice, whereas 200 EpCAM⁻ cells produced only 1 tumor among 10 injected mice at 6 weeks after transplantation, and the tumor sizes were much larger in the EpCAM⁺ cells than in the EpCAM⁻

cells (Figure 5*B* and Supplementary Figure 3*E*; see supplementary material online at www.gastrojournal.org). EpCAM$^+$ cells produced tumors with a mixture of both EpCAM$^+$ and EpCAM$^-$ cells in xenografts, and these cells invaded in the capsule and muscles of the leg adjacent to the tumor (Figure 5*C*). EpCAM$^+$ cells derived from tumors again maintained their tumor-initiating capacity, tumor morphology, and invasive ability in an in vivo serial transplantation experiment (Figure 5*D*). Occasionally, EpCAM$^-$ cell fractions produced a few small tumors that always contained a mixture of EpCAM$^+$ and EpCAM$^-$ cells (data not shown), indicating that the contaminated EpCAM$^+$ cells from FACS sorting contribute to the tumor-initiating ability.

To further validate whether EpCAM$^+$ HCC cells were tumor-initiating cells, we isolated EpCAM$^+$ HCC cells from 2 cases of AFP$^+$ (>600 ng/mL serum AFP) HCC clinical specimens using MACS. Consistently, 1×10^4 EpCAM$^+$ cells could induce tumors in NOD/SCID mice, but up to 1×10^6 EpCAM$^-$ cells failed to do so (Table 1). In addition, similar to HCC cell lines, fresh EpCAM$^+$ tumor cells from 2 clinical HCC specimens were more efficient in forming spheroids in vitro than EpCAM$^-$ cells (Supplementary Figure 4; see supplementary material online at www.gastrojournal.org).

FACS analysis results indicate that a majority of EpCAM$^+$ cells express CD133 in HuH7 cells but not in HuH1 cells (Figure 2*B*), which prompted us to compare the tumorigenic capacity of EpCAM$^+$ and CD133$^+$ cells in these cell lines. Noticeably, EpCAM$^+$ HuH1 cells showed marked tumor-initiating capacity compared with CD133$^+$ HuH1 cells (Figure 5*E* and *F*), whereas EpCAM$^+$ and CD133$^+$ cells had similar tumorigenic ability in HuH7 cells (data not shown).

GSK-3β Inhibition Augments EpCAM$^+$ HCC Cells

To determine the role of Wnt/β-catenin signaling[28] in EpCAM$^+$ HCC cells (Figure 1*B*), we first treated HuH1, HuH7, and HLF cells with a GSK-3β inhibitor BIO (Figure 6*A*), which activates Wnt/β-catenin signaling (Figure 6*B*) and maintains undifferentiation of embryonic stem cells.[38] 6-bromoindirubin-3′-oxime (BIO) increased the EpCAM$^+$ cell population in HuH1 and HuH7 cells when compared with the control methylated BIO (MeBIO) (Figure 6*A*). In contrast, BIO had no effect on the CD90$^+$ cell population, which is more tumorigenic than the CD90$^-$ cell population in HLF (Figure 6*A* and data not shown). Enrichment of EpCAM$^+$ cells was provoked further by the treatment of Wnt10B-conditioned media in HuH7 cells (Figure 6*C*).[34] BIO induced morphologic alteration of HuH7 cells because most cells became small and round when compared with MeBIO and suppressed EpCAM$^-$ AFP$^-$ cell populations (Figure 6*D*). Moreover, BIO induced *TACSTD1*, *MYC*, and *hTERT* expression and spheroid formation (Figure 6*E* and *F*).

Table 1. The Tumor-Initiating Capacity of EpCAM$^+$ Cells From Clinical HCC Specimens

HCC patients				Tumor incidence (mice with tumors/total no. of mice injected)	
No.	% of EpCAM$^+$ HCC cells	Groups	No. of cells injected	2 months	3 months
1	5.2	EpCAM$^+$	1×10^3	0/3	0/3
			1×10^4	2/3	2/3
			1×10^5	2/2	2/2
		EpCAM$^-$	1×10^5	0/3	0/3
			1×10^6	0/2	0/2
2	1.4	EpCAM$^+$	1×10^3	0/2	0/2
			1×10^4	0/1	1/1
		EpCAM$^-$	1×10^4	0/3	0/3
			1×10^5	0/2	0/2

EpCAM Blockage by RNA Interference

One of the hallmarks of CSCs is its resistance to conventional chemotherapeutic agents resulting in tumor relapse and thus targeting CSCs is critical to achieve successful tumor remission. Consistently, 5-FU could increase the EpCAM$^+$ population and spheroid formation of HuH1 and HuH7 cells (Figure 7*A* and *B*) (data not shown), suggesting a differential sensitivity of EpCAM$^+$ and EpCAM$^-$ HCC cells to 5-FU. In contrast, EpCAM blockage via RNA interference dramatically decreased the population of EpCAM$^+$ cells (Figure 7*C*), and significantly inhibited cellular invasion, spheroid formation, and tumorigenicity of HuH1 cells (Figure 7*D–F*). Thus, EpCAM may serve as a molecular target to eliminate HCC cells with stem/progenitor cell features.

Discussion

The cellular origin of HCC is currently in debate. In this study, we found that EpCAM can serve as a marker to enrich HCC cells with tumor-initiating ability and with some stem/progenitor cell traits. EpCAM is expressed in many human cancers with an epithelial origin.[39] During embryogenesis, EpCAM is expressed in fertilized oocytes, embryonic stem cells, and embryoid bodies, suggesting its role in early stage embryogenesis.[40] Furthermore, a recent article indicated that EpCAM is expressed in colonic and breast CSCs.[41] Taken together, these data suggest a critical role of EpCAM in CSCs as well as embryonic and somatic stem cells. Consistently, we found that EpCAM expression is regulated by Wnt/β-catenin signaling[29] and tumorigenic and highly invasive HpSC-HCC is orchestrated by a subset of cells expressing EpCAM and AFP with stem cell-like features and self-renewal and differentiation capabilities regulated by Wnt/β-catenin signaling (this study). Thus, EpCAM may be a common gene expressed in undifferentiated normal cells and HCCs with activated Wnt/β-catenin signaling. It may act as a downstream molecule

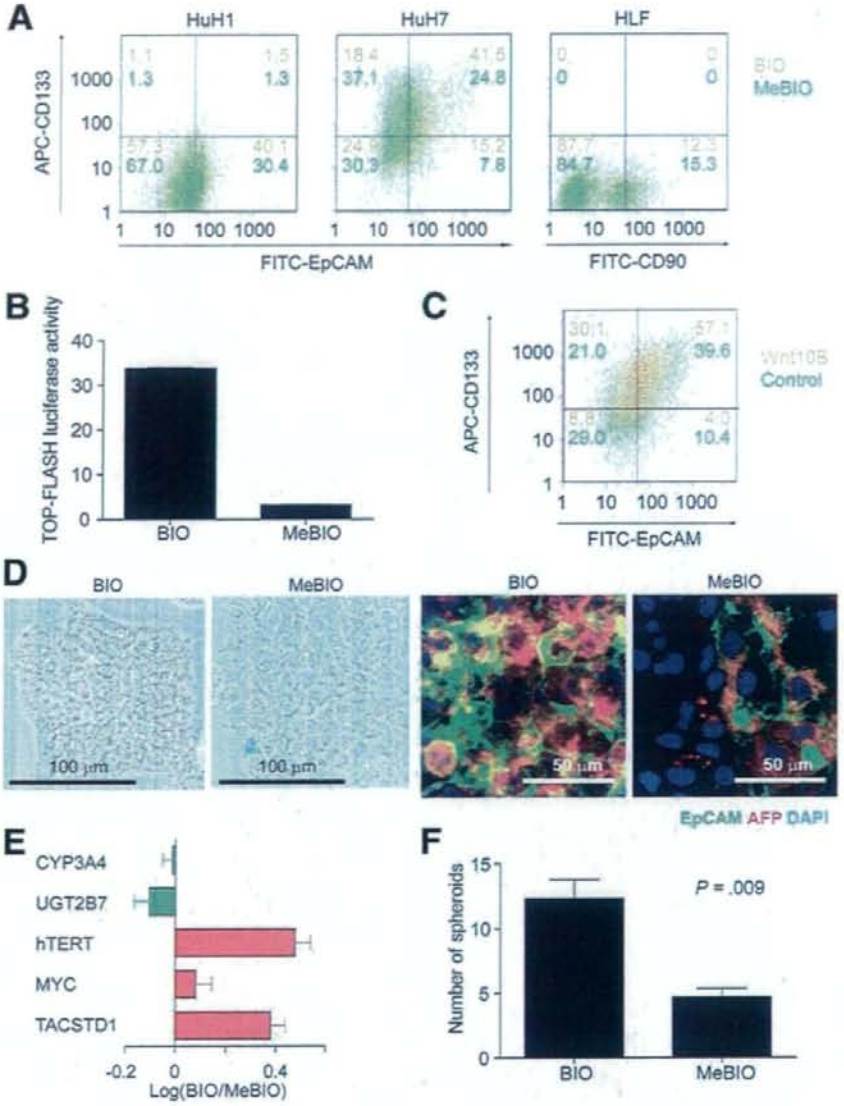

Figure 6. Wnt/β-catenin signaling augments EpCAM⁺ HCC cells. (A) Flow cytometer analysis of HuH1, HuH7, and HLF cells treated with 2 μmol/L of BIO (orange) or MeBIO (green) for 10 days and stained with anti-EpCAM, anti-CD133 and anti-CD90 antibodies. (B) TOP-FLASH luciferase assays of HuH7 cells treated with 2 μmol/L of BIO or MeBIO. (C) Flow cytometer analysis of HuH7 cells cultured in normal media (Dulbecco's modified Eagle medium supplemented with 10% FBS) or Wnt10B conditioned media (details are described in the Materials and Methods section). Cells were cultured in each medium for 2 weeks. (D) Representative phase-contrast images (left panel: scale bar, 100 μm) or IF images (right panel: scale bar, 50 μm) of HuH7 cells treated with 2 μmol/L of BIO or MeBIO for 14 days. (E) Quantitative reverse transcription-polymerase chain reaction analysis of representative HpSC-HCC–related genes in HuH7 cells treated with 2 μmol/L of BIO or MeBIO for 14 days. (F) Spheroid formation assay of HuH7 cells treated with 2 μmol/L of BIO or MeBIO for 14 days (mean ± SD). FITC, fluorescein isothiocyanate.

to maintain HCC stemness and serve as a good marker for HCC initiating cells.

CD133 or CD90 have been used to identify potential hepatic CSCs.[35,42] CD133 is expressed in normal and malignant stem cells of the neural, hematopoietic, epithelial, hepatic, and endothelial lineages,[23,43,44] suggesting that CD133 is also a common marker to detect normal cells and CSCs. Captivatingly, EpCAM expression overlaps with CD133 expression in normal human colon tissues and colorectal cancer tissues, yet CD133⁺ and CD133⁻ cells are equally tumorigenic.[45] Similarly, we found that EpCAM⁺ and EpCAM⁻ HuH1 cells equally expressed CD133, but only EpCAM⁺ cells developed large hypervascular tumors. Our data suggest that EpCAM may be a better marker than CD133 to enrich HCC tumor-initiating cells from AFP⁺ tumors. We also found that CD90 expression was limited to HCC cell lines that are EpCAM⁻ AFP⁻, and Wnt/β-catenin signaling had little effect on CD90⁺ cell enrichment. These results suggest that the expression patterns of various stem cell markers in tumor-initiating cells with stem/progenitor cell features may be different in each HCC subtype, possibly owing to the heterogeneity of activated signaling pathways in normal stem/progenitor cells where these tumor-initiating cells may originate. Therefore, it would be useful to

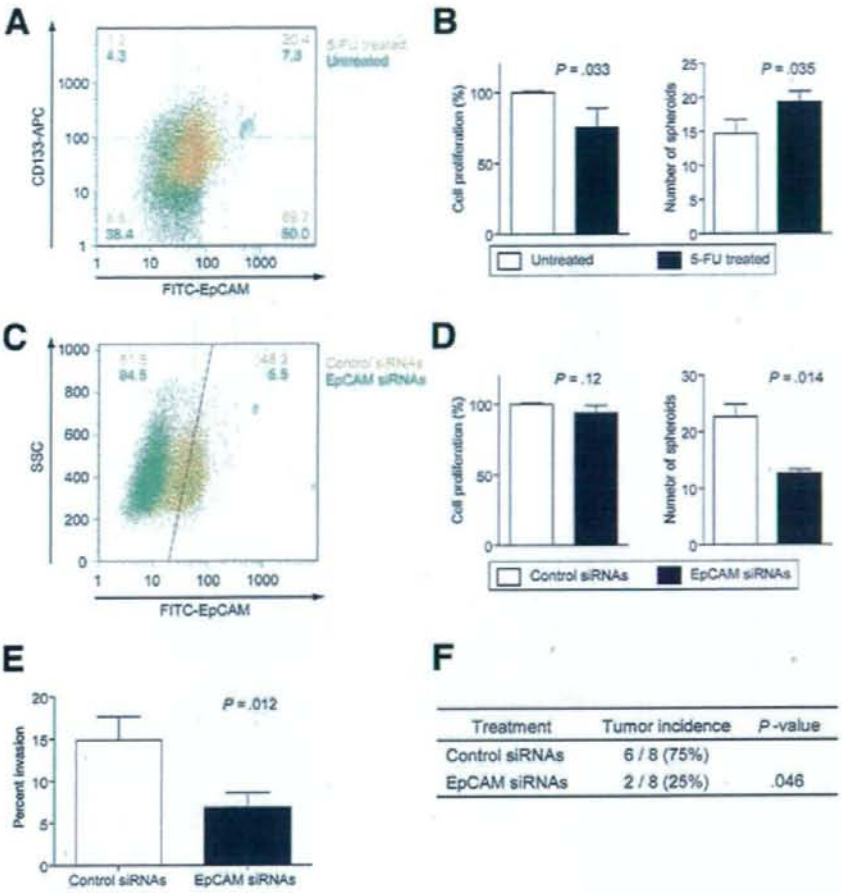

Treatment	Tumor incidence	P-value
Control siRNAs	6 / 8 (75%)	
EpCAM siRNAs	2 / 8 (25%)	.046

Figure 7. EpCAM blockage inhibits the tumorigenic and invasive capacity of EpCAM$^+$ HCC cells. (A) Enrichment of EpCAM$^+$ cells after 5-FU treatment. HuH1 cells refer as control or without treatment (green) or treated with 2 μg/mL of 5-FU (orange) for 3 days and analyzed by FACS using anti-EpCAM and anti-CD133 antibodies. (B) Spheroid formation of HuH1 cells treated with 2 μg/mL of 5-FU for 3 days. (C) FACS analysis of HuH1 cells treated with a control siRNA (orange) or EpCAM-specific siRNA (green) at day 3 after transfection. (D) Spheroid formation or (E) invasive capacity ofEpCAM$^+$ HuH1 cells transfected with a control siRNA or EpCAM-specific siRNA. Experiments were performed in triplicate and the data are shown as mean ± SD. (D) siRNAs. (F) Inhibition of tumor formation in vivo by EpCAM gene silencing. EpCAM$^+$ HuH1 cells were transfected with siRNA oligos and 1000 cells were injected 24 hours after transfection.

comprehensively investigate the expression patterns of stem cell markers to characterize the population of CSCs that may correlate with the activation of their distinct molecular pathways.

CSCs may be more resistant to chemotherapeutic agents than differentiated tumor cells possibly owing to an increased expression of adenosine triphosphate-binding cassette transporters and anti-apoptotic proteins.[4] Thus, the development of an effective strategy to target CSC pools together with conventional chemotherapies is essential to eradicate a tumor mass.[14] By blocking the programs that activate self-renewal and/or inhibit asymmetric division, CSC features could be destemmed.[46,47] Consistently, EpCAM blockage could inhibit cellular invasion and tumorigenicity of EpCAM$^+$ HCC cells, revealing the feasibility of targeting a CSC marker to destem CSC features. EpCAM may induce c-Myc,[48] a common molecular node activated in HpSC-HCC.[27] c-Myc, together with Oct3/4, Sox2, and Klf4, can induce pluripotent stem cells from adult fibroblasts.[49] It is possible that EpCAM blockage to inhibit hepatic CSCs may result in a suppression of c-Myc signaling. Encouragingly, EpCAM-specific antibodies are currently in phase II clinical trials.[50] Furthermore, a recent study indicated that EpCAM$^+$ circulating tumor cells identified by a unique microfluidic platform can be used to monitor outcomes of patients undergoing systemic treatment.[51] Therefore, it may be useful to combine EpCAM antibodies with conventional chemotherapy to target both CSCs and non-CSCs for the treatment of HCC.

Supplementary Data

Note: To access the supplementary material accompanying this article, visit the online version of *Gastroenterology* at www.gastrojournal.org, and at doi: 10.1053/j.gastro.2008.12.004.

References

1. Fialkow PJ. Clonal origin of human tumors. Biochim Biophys Acta 1976;458:283–321.

2. Heppner GH. Tumor heterogeneity. Cancer Res 1984;44:2259–2265.
3. Hanahan D, Weinberg RA. The hallmarks of cancer. Cell 2000;100:57–70.
4. Jordan CT, Guzman ML, Noble M. Cancer stem cells. N Engl J Med 2006;355:1253–1261.
5. Clarke MF, Dick JE, Dirks PB, et al. Cancer stem cells—perspectives on current status and future directions: AACR Workshop on cancer stem cells. Cancer Res 2006;66:9339–9344.
6. Potter VR. Phenotypic diversity in experimental hepatomas: the concept of partially blocked ontogeny. The 10th Walter Hubert Lecture. Br J Cancer 1978;38:1–23.
7. Sell S. Cellular origin of cancer: dedifferentiation or stem cell maturation arrest? Environ Health Perspect 1993;101(Suppl 5):15–26.
8. Wicha MS, Liu S, Dontu G. Cancer stem cells: an old idea—a paradigm shift. Cancer Res 2006;66:1883–1890.
9. Al Hajj M, Wicha MS, Benito-Hernandez A, et al. Prospective identification of tumorigenic breast cancer cells. Proc Natl Acad Sci U S A 2003;100:3983–3988.
10. Singh SK, Hawkins C, Clarke ID, et al. Identification of human brain tumour initiating cells. Nature 2004;432:396–401.
11. Bonnet D, Dick JE. Human acute myeloid leukemia is organized as a hierarchy that originates from a primitive hematopoietic cell. Nat Med 1997;3:730–737.
12. Ricci-Vitiani L, Lombardi DG, Pilozzi E, et al. Identification and expansion of human colon-cancer-initiating cells. Nature 2007;445:111–115.
13. O'Brien CA, Pollett A, Gallinger S, et al. A human colon cancer cell capable of initiating tumour growth in immunodeficient mice. Nature 2007;445:106–110.
14. Dean M, Fojo T, Bates S. Tumour stem cells and drug resistance. Nat Rev Cancer 2005;5:275–284.
15. Rich JN. Cancer stem cells in radiation resistance. Cancer Res 2007;67:8980–8984.
16. Parkin DM, Bray F, Ferlay J, et al. Global cancer statistics, 2002. CA Cancer J Clin 2005;55:74–108.
17. Sell S, Pierce GB. Maturation arrest of stem cell differentiation is a common pathway for the cellular origin of teratocarcinomas and epithelial cancers. Lab Invest 1994;70:6–22.
18. Thorgeirsson SS, Grisham JW. Hepatic stem cells. Semin Liver Dis 2003;23:301.
19. Thorgeirsson SS, Grisham JW. Molecular pathogenesis of human hepatocellular carcinoma. Nat Genet 2002;31:339–346.
20. Lee JS, Heo J, Libbrecht L, et al. A novel prognostic subtype of human hepatocellular carcinoma derived from hepatic progenitor cells. Nat Med 2006;12:410–416.
21. Sigal SH, Brill S, Fiorino AS, et al. The liver as a stem cell and lineage system. Am J Physiol 1992;263:G139–G148.
22. Schmelzer E, Wauthier E, Reid LM. The phenotypes of pluripotent human hepatic progenitors. Stem Cells 2006;24:1852–1858.
23. Schmelzer E, Zhang L, Bruce A, et al. Human hepatic stem cells from fetal and postnatal donors. J Exp Med 2007;204:1973–1987.
24. Dan YY, Riehle KJ, Lazaro C, et al. Isolation of multipotent progenitor cells from human fetal liver capable of differentiating into liver and mesenchymal lineages. Proc Natl Acad Sci U S A 2006;103:9912–9917.
25. Zaret KS. Regulatory phases of early liver development: paradigms of organogenesis. Nat Rev Genet 2002;3:499–512.
26. Shafritz DA, Oertel M, Menthena A, et al. Liver stem cells and prospects for liver reconstitution by transplanted cells. Hepatology 2006;43:S89–S98.
27. Yamashita T, Forgues M, Wang W, et al. EpCAM and alpha-fetoprotein expression defines novel prognostic subtypes of hepatocellular carcinoma. Cancer Res 2008;68:1451–1461.
28. Reya T, Clevers H. Wnt signalling in stem cells and cancer. Nature 2005;434:843–850.
29. Yamashita T, Budhu A, Forgues M, et al. Activation of hepatic stem cell marker EpCAM by Wnt-β-catenin signaling in hepatocellular carcinoma. Cancer Res 2007;67:10831–10839.
30. Budhu A, Forgues M, Ye QH, et al. Prediction of venous metastases, recurrence and prognosis in hepatocellular carcinoma based on a unique immune response signature of the liver microenvironment. Cancer Cell 2006;10:99–111.
31. Ye QH, Qin LX, Forgues M, et al. Predicting hepatitis B virus-positive metastatic hepatocellular carcinomas using gene expression profiling and supervised machine learning. Nat Med 2003;9:416–423.
32. Wu CG, Forgues M, Siddique S, et al. SAGE transcript profiles of normal primary human hepatocytes expressing oncogenic hepatitis B virus X protein. FASEB J 2002;16:1665–1667.
33. Kubota H, Reid LM. Clonogenic hepatoblasts, common precursors for hepatocytic and biliary lineages, are lacking classical major histocompatibility complex class I antigen. Proc Natl Acad Sci U S A 2000;97:12132–12137.
34. Yoshikawa H, Matsubara K, Zhou X, et al. WNT10B functional dualism: beta-catenin/Tcf-dependent growth promotion or independent suppression with deregulated expression in cancer. Mol Biol Cell 2007;18:4292–4303.
35. Yang ZF, Ho DW, Ng MN, et al. Significance of CD90(+) cancer stem cells in human liver cancer. Cancer Cell 2008;13:153–166.
36. Dontu G, Abdallah WM, Foley JM, et al. In vitro propagation and transcriptional profiling of human mammary stem/progenitor cells. Genes Dev 2003;17:1253–1270.
37. Fang D, Nguyen TK, Leishear K, et al. A tumorigenic subpopulation with stem cell properties in melanomas. Cancer Res 2005;65:9328–9337.
38. Sato N, Meijer L, Skaltsounis L, et al. Maintenance of pluripotency in human and mouse embryonic stem cells through activation of Wnt signaling by a pharmacological GSK-3-specific inhibitor. Nat Med 2004;10:55–63.
39. Balzar M, Winter MJ, de Boer CJ, et al. The biology of the 17-1A antigen (Ep-CAM). J Mol Med 1999;77:699–712.
40. Trzpis M, McLaughlin PM, de Leij LM, et al. Epithelial cell adhesion molecule: more than a carcinoma marker and adhesion molecule. Am J Pathol 2007;171:386–395.
41. Dalerba P, Dylla SJ, Park IK, et al. Phenotypic characterization of human colorectal cancer stem cells. Proc Natl Acad Sci U S A 2007;104:10158–10163.
42. Ma S, Chan KW, Hu L, et al. Identification and characterization of tumorigenic liver cancer stem/progenitor cells. Gastroenterology 2007;132:2542–2556.
43. Yin AH, Miraglia S, Zanjani ED, et al. AC133, a novel marker for human hematopoietic stem and progenitor cells. Blood 1997;90:5002–5012.
44. Fargeas CA, Corbeil D, Huttner WB. AC133 antigen, CD133, prominin-1, prominin-2, etc.: prominin family gene products in need of a rational nomenclature. Stem Cells 2003;21:506–508.
45. Shmelkov SV, Butler JM, Hooper AT, et al. CD133 expression is not restricted to stem cells, and both CD133+ and CD133- metastatic colon cancer cells initiate tumors. J Clin Invest 2008;118:2111–2120.
46. Hill RP, Perris R. "Destemming" cancer stem cells. J Natl Cancer Inst 2007;99:1435–1440.
47. Piccirillo SG, Reynolds BA, Zanetti N, et al. Bone morphogenetic proteins inhibit the tumorigenic potential of human brain tumour-initiating cells. Nature 2006;444:761–765.
48. Munz M, Kieu C, Mack B, et al. The carcinoma-associated antigen EpCAM upregulates c-myc and induces cell proliferation. Oncogene 2004;23:5748–5758.

49. Takahashi K, Tanabe K, Ohnuki M, et al. Induction of pluripotent stem cells from adult human fibroblasts by defined factors. Cell 2007;131:861–872.
50. Chaudry MA, Sales K, Ruf P, et al. EpCAM an immunotherapeutic target for gastrointestinal malignancy: current experience and future challenges. Br J Cancer 2007;96:1013–1019.
51. Nagrath S, Sequist LV, Maheswaran S, et al. Isolation of rare circulating tumour cells in cancer patients by microchip technology. Nature 2007;450:1235–1241.

Received March 9, 2008. Accepted December 1, 2008.

Reprint requests

Address requests for reprints to: Xin Wei Wang, PhD, Liver Carcinogenesis Section, Laboratory of Human Carcinogenesis, Center for Cancer Research, National Cancer Institute, 37 Convent Drive, Building 37, Room 3044A, MSC 4258, Bethesda, Maryland 20892-4258. e-mail: xw3u@nih.gov; fax: (301) 496-0497.

Acknowledgments

Microarray data are available publicly at http://www.ncbi.nlm.nih.gov/geo/ (accession number: GSE5975).

The authors thank Drs Curtis Harris and Sharon Pine for critical readings of the manuscript; Ms Barbara Taylor and Dr Susan Garfield for technical assistance; Drs Ali Brivanlou (Rockefeller University), Steve Strom (University of Pittsburgh), and Bert Vogelstein (Johns Hopkins University) for generously providing their research materials.

Conflicts of interest

The authors disclose no conflicts.

Funding

The authors disclose the following: This work was supported in part by the Intramural Research Program of the Center for Cancer Research, the US National Cancer Institute. Dr Yang, Dr HY Wang, Dr Jia, Dr Ye, Dr Qin, and Dr Tang were supported by research grants from the China National Natural Science Foundation for Distinguished Young Scholars (30325041) and the China National "863" R&D High-Tech Key Project (2002BA711A02-4). Dr Reid was supported by a sponsored research grant from Vesta Therapeutics (Research Triangle Park, NC), National Institutes of Health grants (R01 AA014243 and R01 IP30-DK065933), and a US Department of Energy grant (DE-FG02-02ER-63477). Sponsors had no role in the study design, data collection, analysis, and interpretation. Dr Yamashita, Dr Ji, Dr Budhu, Dr Forgues, Dr Yang, Dr Wang, Dr Jia, Dr Ye, Dr Wauthier, Dr Minato, Dr Honda, Dr Kaneko, and Dr Wang disclose no conflicts.

Supplementary Materials and Methods

FACS and MACS Analyses

Cultured cells were trypsinized, washed, and resuspended in Hank's balanced salt solutions (Lonza, Basel, Switzerland) supplemented with 1% HEPES and 2% fetal bovine serum. Cells then were incubated with FITC-conjugated anti-EpCAM monoclonal antibody Clone Ber-EP4 (DAKO, Carpinteria, CA) on ice for 30 minutes, and $EpCAM^+$ and $EpCAM^-$ cells were isolated by a BD FACSAria cell sorting system (BD Biosciences). For magnetic separation, cells were labeled 24 hours after enzymatic dissociation with primary EpCAM antibody (mouse IgG1; Dako), subsequently magnetically labeled with rat anti-mouse IgG1 Microbeads, and separated on a MACS LS column (Miltenyi Biotec, Inc, Auburn, CA). All the procedures were performed according to the manufacturer's instructions. The purity of sorted cells was evaluated by FACS. Fixed cells also were analyzed by FACS using a FACSCalibur (BD Biosciences). Anti-EpCAM antibody VU-1D9, anti-CD133/2 clone 293C3 (Miltenyi Biotec Inc), and anti-CD90 clone 5E10 (StemCell Technologies Inc, Vancouver, British Columbia, Canada) were used to detect $EpCAM^+$, $CD133^+$, or $CD90^+$ cells. Intracellular AFP levels were examined by a BD Cytofix/Cytoperm Fixation/Permeabilization Kit (San Jose, CA) and anti-AFP rabbit polyclonal antibody (DAKO).

Quantitative Reverse Transcription–Polymerase Chain Reaction and IHC Analyses

Total RNA was extracted using TRIzol (Invitrogen) according to the manufacturer's instructions. The expression of selected genes was determined in triplicate using the Applied Biosystems 7500 Sequence Detection System (Applied Biosystems, Foster City, CA) as previously described.[1] Genes expressed in embryonic stem cells were determined in quadruplicate using TaqMan Human Stem Cell Pluripotency Array (Applied Biosystems). IHC analyses with specific antibodies were performed essentially as previously described.[1] Confocal fluorescence microscopic analysis was performed essentially as previously described.[2]

References

1. Yamashita T, Forgues M, Wang W, et al. EpCAM and alpha-fetoprotein expression defines novel prognostic subtypes of hepatocellular carcinoma. Cancer Res 2008;68:1451–1461.
2. Wang W, Budhu A, Forgues M, et al. Temporal and spatial control of nucleophosmin by the Ran-Crm1 complex in centrosome duplication. Nat Cell Biol 2005;7:823–830.

Supplemetary Table 1. Clinicopathologic Characteristics of HpSC-HCC and MH-HCC Cases Used for Oligonucleotide Microarray Analyses

Parameters	HpSC-HCC (n = 60)	MH-HCC (n = 96)	*P* value[a]
Mean age, *y* (SD)	46.0 ± 10.7	52.9 ± 10.5	.0004
Sex: male/female	50/10	87/9	.18
Cirrhosis: yes/no/no data	56/4	88/7/1	.72
Median AFP level, *ng/mL* (25%–75%)	1706 (865–5915)	11.8 (4.0–48.6)	<.0001
Histologic grade[b]			
I–II	14	41	
II–III	44	48	
III–IV	2	5	
No data	0	2	.031
Mean tumor size, *cm* (SD)	5.1 ± 3.0	4.4 ± 3.0	.088
Multinodular: yes/no	16/44	15/81	.09
Portal vein invasion, yes/no[c]	11/49	9/87	.10
TNM classification			
I	24	46	
II	22	42	
III	14	8	.03
Virus status: HBV/HBV + HCV/unknown	56/4/0	95/0/1	.43

[a]Mann–Whitney *U* test or χ^2 test.
[b]Edmondson–Steiner.
[c]Macroscopic portal vein invasion.

Supplementary Table 2. Clinicopathologic Characteristics of HpSC-HCC and MH-HCC Cases Used for IHC

Parameters	HpSC-HCC (n = 24)	MH-HCC (n = 55)	*P* value[a]
Mean age, *y* (SD)	46.4 ± 9.4	58.4 ± 11.9	<.0001
Sex: male/female	20/4	48/7	.64
Cirrhosis: yes/no	23/1	46/9	.14
Median AFP level, *ng/mL* (25%–75%)	1620 (887–3166)	12 (9.3–219)	<.0001
Histologic grade[b]			
I–II	12	32	
II–III	8	21	
III–IV	4	2	.13
Mean tumor size, *cm* (SD)	7.1 ± 3.6	5.2 ± 3.6	.014
Multinodular: yes/no	4/20	16/39	.24
Portal vein invasion: yes/no[c]	12/12	12/43	.012
TNM classification			
I	4	19	
II	8	20	
III	12	16	.14
Virus status: HBV/HCV/unknown	21/2/1	32/21/2	.026

[a]Mann–Whitney *U* test or χ^2 test.
[b]Edmondson–Steiner.
[c]Macroscopic portal vein invasion.

Supplementary Table 3. Top 10 List of Canonical Pathways Activated in HpSC-HCC From Ingenuity Pathway Analysis

Pathways	Genes included in cluster A
Axonal guidance signaling	
Up	ROBO2, ARPC5L (includes EG:81873), SEMA4G, PDGFRB, PLCB1, PRKCD, FGFR3, FZD5, MERTK, DDR1, LINGO1, SEMA3C
Down	PIK3C3, IGF1, PIK3C2G, MAP2K2, ARHGEF15
Transforming growth factor-β signaling	
Up	PDGFRB, FGFR3, MERTK, UBD, DDR1, SMAD5
Down	MAP2K2, HNF4A
Integrin signaling	
Up	ARPC5L (includes EG:81873), PDGFRB, FGFR3, GRB7, MERTK, ITGB5, DDR1, DDEF1
Down	PIK3C3, MYLK, PIK3C2G, MAP2K2
Apoptosis signaling	
Up	PDGFRB, BAK1, CYCS, FGFR3, MERTK, DDR1
Down	MAP3K5, MAP2K2
G2/M DNA damage checkpoint regulation	
Up	YWHAZ, CCNB2, UBD, WEE1
Down	CDKN2A, GADD45A
ERK/MAPK signaling	
Up	ELF3, PDGFRB, YWHAZ, PRKCD, FGFR3, MERTK, DDR1
Down	PIK3C3, DUSP1, PIK3C2G, ESR1, MAP2K2
Wnt/β-catenin signaling	
Up	DKK1, SOX9, FZD5, UBD, TCF7L2, CSNK1E
Down	CDKN2A, RARG
PI3K/AKT signaling	
Up	PDGFRB, YWHAZ, FGFR3, MERTK, DDR1
Down	MAP3K5, MAP2K2, GYS2
Amyloid processing	
Up	BACE2, CSNK1E, MAPK13
Down	
Leukocyte extravasation signaling	
Up	PRKCD, CLDN4, CLDN1, MMP11, MAPK13
Down	PIK3C3, CLDN2, PIK3C2G, MAP2K2

NOTE. The top 10 pathways were selected based on the significance for the enrichment of the genes with a particular canonical signaling pathway determined by the one-sided Fisher exact test ($P < .01$).

Supplementary Table 4. Top 10 List of Canonical Pathways Activated in MH-HCC From Ingenuity Pathway Analysis

Pathways	Genes included in cluster B
Lipopolysaccharide/interleukin-1–mediated inhibition of RXR function	
Up	SULT1C2, ACSL4, ACSL3, FABP5, GSTP1
Down	NR1I2, NR1I3, CYP7A1, ALDH1L1, ABCB1, SLC10A1, SLC27A2, CD14, GSTM1, ALDH6A1, GSTM4, ACSL5, CES2 (includes EG:8824), FMO3, SULT2A1 (includes EG:6822), GSTA1, CYP2C8, LC27A5, CYP3A7, ABCG5, ALDH8A1, APOC4 (includes EG:346), CYP3A4, ACSL1, ABCB11, FMO4, MAOA
Xenobiotic metabolism signaling	
Up	SULT1C2, PRKCD, GSTP1, MAPK13
Down	NR1I2, NR1I3, ALDH1L1, ABCB1, UGT2B15, MAP2K2, UGT2B7, PPARGC1A, GSTM1, PIK3C3, ALDH6A1, GSTM4, CES2 (includes EG:8824), MAP3K5, FMO3, PIK3C2G, SULT2A1 (includesEG:6822), CYP1A2, GSTA1, CYP2C8, CYP3A7, NQO2, ALDH8A1, CYP3A4, CES1 (includes EG:1066), FMO4, MAOA
Hepatic cholestasis	
Up	ADCY3, PRKCD
Down	CD14, ABCG5, NR1I2, CYP7A1, CYP7B, CYP8B1, ABCB1, ESR1, SLC10A1, ABCB11, ABCB4, HNF4A
Aryl hydrocarbon receptor signaling	
Up	GSTP1
Down	CDKN2A, NQO2, GSTM1, ALDH8A1, ALDH6A1, ALDH1L1, GSTM4, ESR1, CYP1A2, GSTA1, RARG
NRF2-mediated oxidative stress response	
Up	DNAJA4, PRKCD, GSTP1
Down	NQO2, GSTM1, AOX1, PIK3C3, GSTM4, MAP3K5, SOD1, PIK3C2G, MAP2K2, FKBP5, GSTA1
Complement system	
Up	
Down	C8A, C1R, MASP1, C6, C8B, MASP2
Coagulation system	
Up	
Down	SERPINC1, KLKB1, F9, KNG1 (includes EG:3827), F11
Acute-phase response signaling	
Up	MAPK13
Down	APCS, RBP5, C1R, MAP3K5, HRG, MAP2K2, KLKB1, SAA4
p53 signaling	
Up	THBS1
Down	CDKN2A, PIK3C3, SNAI2, GADD45A, PIK3C2G, GADD45B
LXR/RXR activation	
Up	HMGCR
Down	CD14, ABCG5, APOA5, CYP7A1, APOC4 (includes EG:346)

LXR/RXR, liver X receptor/retinoid X receptor; NRF2, NF-E2-related factor 2.
NOTE. The top 10 pathways were selected based on the significance for the enrichment of the genes with a particular canonical signaling pathway determined by the one-sided Fisher exact test ($P < .01$).

Common Transcriptional Signature of Tumor-Infiltrating Mononuclear Inflammatory Cells and Peripheral Blood Mononuclear Cells in Hepatocellular Carcinoma Patients

Yoshio Sakai, Masao Honda, Haruo Fujinaga, Isamu Tatsumi, Eishiro Mizukoshi, Yasunari Nakamoto, and Shuichi Kaneko

Department of Gastroenterology, Kanazawa University, School of Medicine, Kanazawa, Japan

Abstract

Hepatocellular carcinoma (HCC) is frequently associated with infiltrating mononuclear inflammatory cells. We performed laser capture microdissection of HCC-infiltrating and noncancerous liver-infiltrating mononuclear inflammatory cells in patients with chronic hepatitis C (CH-C) and examined gene expression profiles. HCC-infiltrating mononuclear inflammatory cells had an expression profile distinct from noncancerous liver-infiltrating mononuclear inflammatory cells; they differed with regard to genes involved in biological processes, such as antigen presentation, ubiquitin-proteasomal proteolysis, and responses to hypoxia and oxidative stress. Immunohistochemical analysis and gene expression databases suggested that the up-regulated genes involved macrophages and Th1 and Th2 CD4 cells. We next examined the gene expression profile of peripheral blood mononuclear cells (PBMC) obtained from CH-C patients with or without HCC. The expression profiles of PBMCs from patients with HCC differed significantly from those of patients without HCC ($P < 0.0005$). Many of the up-regulated genes in HCC-infiltrating mononuclear inflammatory cells were also differentially expressed by PBMCs of HCC patients. Analysis of the commonly up-regulated or down-regulated genes in HCC-infiltrating mononuclear inflammatory cells and PBMCs of HCC patients showed networks of nucleophosmin, SMAD3, and proliferating cell nuclear antigen that are involved with redox status, the cell cycle, and the proteasome system, along with immunologic genes, suggesting regulation of anticancer immunity. Thus, exploring the gene expression profile of PBMCs may be a surrogate approach for the assessment of local HCC-infiltrating mononuclear inflammatory cells. [Cancer Res 2008;68(24):10267–79]

Introduction

Hepatocellular carcinoma (HCC) is one of the most frequent malignancies worldwide (1). It commonly develops from chronic liver diseases, such as viral hepatitis (2) and chronic hepatitis, resulting from hepatitis C virus (HCV) infection, is a major risk factor. Indeed, 7% of patients with liver cirrhosis (LC) caused by persistent HCV (LC-C) infection develop HCC annually (3).

Cancer tissues are often associated with infiltrating inflammatory cells, such as tumor-associated macrophages (4), T lymphocytes (5), and antigen-presenting cells (6). These tumor-infiltrating mononuclear inflammatory cells are thought to be important modulators of HCC (7). However, their actual role remains controversial. Increased numbers in HCC have been correlated with a fair prognosis (8), but tumor-infiltrating mononuclear inflammatory cells in HCC tissues have also been found to involve more FOXP3$^+$ regulatory T cells (9) and provide a cancer-favorable environment that leads to resistance to therapy. Characterization of tumor-infiltrating mononuclear inflammatory cells may be valuable in understanding tumor immunology and, possibly, in predicting the prognosis of HCC patients (7).

Peripheral blood mononuclear cells (PBMCs) consist of immune cells, such as monocytes and lymphocytes, and are essential players in the host immune defense system, which responds to various abnormal conditions in the host (10). PBMCs and tumor-infiltrating mononuclear inflammatory cells contain CTLs, specifically cytocidal to cancer tissues (11) and regulatory T cells that can suppress the host immune response against cancer (9). Thus, PBMCs may potentially reflect host immune status. However, there are limited assays for assessing the immune status of PBMCs, such as a proliferation assay, measurements of cytokine production, and the assessment of cytocidal potential.

The advent of cDNA microarray technology for the analysis of gene expression profiles has been useful in comprehensively disclosing underlying molecular features and has provided considerable information for basic science and clinical medicine. We have analyzed gene expression in liver diseases (12, 13) and believe it may become a useful diagnostic tool using liver tissue biopsy samples (14). We have also reported that gene expression profiling of PBMCs predicted the effect of IFN for the eradication of HCV (15) and can provide biomarkers not only for the control of blood sugar but also possibly for predisposing diabetic factors (16). Gene expression profiling of PBMCs from patients with renal cell carcinoma can be used to predict their response to systemic chemotherapy (17). Thus, gene expression information from the cellular components of peripheral blood may be useful in interpreting the internal condition of the patient.

In this study, we used DNA microarray technology to examine differences in gene expression profiles between HCC-infiltrating and noncancerous liver-infiltrating mononuclear inflammatory cells, which were selectively microdissected (12), and the gene expression profiles of PBMCs from LC-C patients with or without HCC. We observed distinct transcriptional features of HCC-infiltrating mononuclear inflammatory cells, reflecting the immune status of the local environment. Intriguingly, the transcriptional features of the HCC-infiltrating mononuclear inflammatory cells were shared with PBMCs from HCC patients. Thus, we suggest the possibility that the gene expression profile of PBMCs may be useful as a clinical surrogate biomarker for the assessment of

Note: Supplementary data for this article are available at Cancer Research Online (http://cancerres.aacrjournals.org/).

Requests for reprints: Shuichi Kaneko, 13-1 Takara-machi, Kanazawa, Ishikawa 920-8641, Japan. Phone: 81-76-265-2233; Fax: 81-76-234-4250; E-mail: skaneko@m-kanazawa.jp.

doi:10.1158/0008-5472.CAN-08-0911

the internal environment of HCC patients with chronic hepatitis C (CH-C) infection.

Materials and Methods

Study subjects. All patients participating in this study had advanced chronic liver disease, cirrhosis, or persistent HCV infection. Twelve patients who developed HCC as a consequence of advanced chronic liver disease related to hepatitis C and who underwent surgical treatment were enrolled (Supplementary Table S1). HCC and noncancerous liver tissues were obtained and frozen. For analysis of gene expression profiles in PBMCs, 32 LC patients without HCC and 30 LC patients with HCC (Supplementary Table S2) were included. Development of HCC was diagnosed by computed tomography (CT) or magnetic resonance imaging with contrast reagents and abdominal angiography with CT imaging in arterial and portal flow phases (18). The pathologic tumor node metastasis classification system of the Liver Cancer Study Group of Japan was used for the staging of HCC. LC was diagnosed by pathologic findings in biopsy specimens where available; otherwise, radiological imaging, platelet counts, serum hyaluronic acid levels, and indocyanine green retention rates were considered for the diagnosis of cirrhosis. The study has been approved by the institutional review board, and informed consent was obtained from all patients enrolled in the study.

Isolation of PBMCs. PBMCs were isolated from heparinized blood samples by Ficoll-Hipaque density gradient centrifugation, as reported previously (15).

Laser capture microdissection. HCC and noncancerous liver tissues obtained during surgery were frozen in optimum cutting temperature compound (Sakura Finetech; ref. 13). All HCC tissues were nodular and clearly separated by noncancerous tissues macroscopically. Cells infiltrating HCC tissues were visualized under a microscope and precisely excised by laser capture microdissection (LCM) using a CRI-337 (Cell Robotics, Inc.), as previously performed (Supplementary Fig. S1A; ref. 12). Cells infiltrating noncancerous tissues of CH-C patients were visualized and excised similarly.

RNA isolation and amplification. Total RNA was isolated from PBMCs or tissue samples using a microRNA isolation kit (Stratagene) in accordance with the supplied protocol with slight modifications. Isolated RNA was then amplified twice using antisense RNA and an Amino Allyl MessageAmp aRNA kit (Ambion), as described previously (13). The reference RNA sample was isolated from the PBMCs of a 29-yr-old healthy male volunteer and was amplified in the same manner. Amplified RNAs from the PBMCs of patients and the healthy volunteer were labeled with Cy5 and Cy3 (Amersham), respectively. Equal amounts of amplified RNAs were hybridized to an oligo-DNA chip (AceGene Human Oligo Chip 30K, Hitachi Software Engineering Co., Ltd.) overnight and were then washed for image scanning.

DNA microarray image analysis. The fluorescence intensity of each spot on the oligo-DNA chip was determined using a DNA Microarray Scan Array G (PerkinElmer). The images obtained were quantified using a DNASIS array (v2.6, Hitachi Software Engineering Co., Ltd). For normalization, the intensity of each spot without oligo-DNA was subtracted from that with oligo-DNA in the same block. A validated spot was determined when the intensity of the spot was within the intensity ± 2 SDs for each block. By calibrating the median to base quantity, the intensities of all spots were adjusted for normalization between Cy5 and Cy3.

Quantitative real-time detection PCR. Real-time detection PCR (RTD-PCR) was performed as previously described (15). Briefly, template cDNA was synthesized from 1 μg of total RNA using SuperScript II RT (Invitrogen). Primer pairs for chemokine (C-C motif) receptor 1 (*Ccr1*), histone acetyltransferase 1 (*Hat1*), mitogen-activated protein kinase kinase 1 interacting protein 1 (*Map2k1ip1*), phosphatidylinositol glycan anchor biosynthesis, class B (*PigB*), toll-like receptor 2 (*Tlr2*), superoxide dismutase 2 (*Sod2*), cytokeratin 8 (*Krt8*), *Krt18*, *Krt19*, and glyceraldehydes-3-phosphate dehydrogenase, as an internal control of expression, were purchased from the TaqMan assay reagents library (Applied Biosystems). Synthesized cDNA was mixed with the TaqMan Universal Master Mix (Applied Biosystems), as well as each primer pair and reaction was performed using ABI PRISM 7900HT. Relative expression level of each gene was calculated compared with that of internal control in each sample. Results are expressed as means ± SE.

Flow cytometry analysis. Flow cytometry analysis was performed as described previously (19). Briefly, isolated PBMCs were incubated in PBS supplemented with 2% bovine serum albumin (Sigma-Aldrich JAPAN K.K.) with antihuman CCR1 and CCR2 antibodies labeled with Alexa Fluor 647 (Becton Dickinson Pharmingen). The fluorescence intensity of the cells was measured using a FACSort (Becton Dickinson).

Immunohistochemistry. Surgically obtained HCC and noncancerous liver tissues were fixed with neutral buffered formalin, embedded in paraffin, cut into 4-μm sections, and mounted on microscope slides. The fixed slides were deparaffinized and subjected to heat-induced epitope retrieval 98°C for 40 min. After blocking endogenous peroxidase activity in the tissue specimen using 3% hydrogen peroxide, the slides were incubated with appropriately diluted primary antibodies, antihuman CD4 or anti-human CD14 mouse monoclonal antibodies (Visionbiosystems Novocastra). The reaction was visualized by the REAL EnVision Detection System (DAKO) followed by counterstaining with hematoxylin.

Statistical analysis. Hierarchical clustering and principal component analysis of gene expression was performed using BRB-ArrayTools.[1] Fisher's exact test was used to examine the significance of hierarchical clustering in the dendrogram. A class prediction was performed by three nearest neighbors, incorporating genes that were differentially expressed at the $P = 0.002$ significance level, as assessed by the random variance t test (BRB-ArrayTools). For genes to analyze in a pathway, we used a P value of <0.05 with 2,000 permutations to avoid underestimating the presence of meaningful signaling pathways that were coordinately up-regulated or down-regulated with subtle differences (13). The cross-validated misclassification rate was computed, and at least 2,000 permutations were performed for a valid permutation P value. The univariate t values for comparing the classes were used as weights. Student's t-test was performed for RTD-PCR data, and P values of <0.05 were deemed to be statistically significant. The population of CCR1-positive or CCR2-positive cells in PBMCs by flow cytometry analysis was tested for differences (with $P < 0.05$) by the Mann-Whitney U-test, using SPSS software (SPSS Japan, Inc.).

Analysis of expression data for biological processes and networks. As for genes significantly up-regulated or down-regulated in HCC-infiltrating mononuclear inflammatory cells compared with noncancerous liver-infiltrating mononuclear inflammatory cells or in PBMCs in LC without HCC compared with LC with HCC at $P < 0.05$, we have performed analysis of the biological processes using the MetaCore software suite (GeneGo), as described previously (13). Possible networks were created according to the list of the differentially expressed genes using the MetaCore database, a unique curated database of human protein-protein and protein-DNA interactions, transcription factors, and signaling, metabolic, and bioactive molecules. The P value was calculated as described previously (13).

Gene expression data of major leukocyte types and analysis of DNA microarray expression data. Gene expression data for leukocytes were retrieved through publicly accessible databases.[2] The gene set database GDS1775, which includes gene expression data for major leukocyte types, was obtained and subjected to one-way clustering analysis using BRB-Array Tools with genes that were up-regulated in HCC-infiltrating mononuclear inflammatory cells for the enrolled cases above.

Results

Gene expression in mononuclear inflammatory cells infiltrating into HCC tissue. HCC is frequently associated with infiltrating mononuclear inflammatory cells (20), and various attempts have been made to understand their biological significance

[1] http://linus.nci.nih.gov/BRB-ArrayTools.html
[2] http://www.ncbi.nlm.nih.gov/geo/

(8, 9, 21). We selectively obtained HCC-infiltrating mononuclear inflammatory cells by LCM and compared their gene expression profiles with those of noncancerous liver-infiltrating mononuclear inflammatory cells obtained in the same way (Supplementary Fig. S1A; Supplementary Table S1). The gene expression profiles of HCC-infiltrating mononuclear inflammatory cells showed that 115, 206, and 773 genes were up-regulated and 52, 114, and 750 genes were down-regulated compared with those of noncancerous liver-infiltrating mononuclear inflammatory cells at P levels of <0.005, <0.01, and <0.05, respectively (Geo accession no.[3] GSE 10461; Supplementary Fig. S1B).

Genes at the $P < 0.05$ level were analyzed with regard to their role in biological processes in HCC-infiltrating mononuclear inflammatory cells compared with noncancerous liver-infiltrating mononuclear inflammatory cells using the MetaCore pathway analysis software. The significant processes, in which the up-regulated genes in HCC-infiltrating mononuclear inflammatory cells were involved, included antigen presentation, an immunologically important process in antigen-presenting cells, such as monocyte/macrophages and dendritic cells (Table 1; ref. 22). The genes involved in this process were the genes for the CD1d molecule and C-type lectin domain family 4 for glycolipid antigen recognition (23, 24) and CD86, an accessory molecule indispensable for provoking an immune response (25), suggesting an activated immune reaction in these cells. The up-regulated genes in HCC-infiltrating mononuclear inflammatory cells were also involved in the ubiquitin-proteasomal proteolysis process, with significant genes, such as those encoding ubiquitin-conjugating enzymes and proteasome subunits. This process is required to eradicate unnecessary proteins, which are ubiquitinated, and then degraded in proteasomes (26). Processes related to the steps of gene expression, such as transcription by RNA polymerase II, mRNA processing, and the process of the cell cycle were also represented in the genes up-regulated in HCC-infiltrating mononuclear inflammatory cells, indicating enhanced cellular activity. Genes involved in the process of double-strand breaks, such as topoisomerase II α4 (27), and proliferating cell nuclear antigen (PCNA; ref. 28) genes involved in responses to hypoxia and oxidative stress, such as thioredoxin, peroxiredoxin, and antioxidant protein, were also up-regulated, suggesting that HCC-infiltrating mononuclear inflammatory cells were in an activated inflammatory status and under hypoxic or oxidative stress, presumably caused by the HCC. Thus, the profile of up-regulated genes in HCC-infiltrating mononuclear inflammatory cells suggested an inflammatory status, possibly triggered by antigenic stimulation of HCC tissues.

Fewer processes were identified for the down-regulated genes. One intriguing process identified was that of integrin-mediated cell matrix adhesion, suggesting that HCC-infiltrating mononuclear inflammatory cells may be less adhesive in the local tissues where they were found (Supplementary Table S3).

Subpopulation analysis of HCC-infiltrating mononuclear inflammatory cells using immunohistochemistry and transcriptional analysis. Tumor-infiltrating mononuclear inflammatory cells consist of a mixed cell population, including macrophages, effector T cells, and regulatory T cells, which have been considered to be both cancer-favorable or cancer-unfavorable (8, 21). HCC-infiltrating and noncancerous liver-infiltrating mononuclear inflammatory cells were immunohistochemically evaluated to examine the characteristics of the subpopulations. CD14-positive monocytes/macrophages were prominent in HCC-infiltrating mononuclear inflammatory cells, whereas they were rarely observed in noncancerous liver-infiltrating mononuclear inflammatory cells (Fig. 1A). CD4-positive helper T cells were observed in both HCC tissues and noncancerous liver tissues, although in noncancerous liver tissues, these cells tended to accumulate within the aggregates of mononuclear inflammatory cells, whereas they seemed to be scattered in HCC-infiltrating mononuclear inflammatory cells (Fig. 1A).

Next, we examined the genes that were significantly up-regulated in HCC-infiltrating mononuclear inflammatory cells compared with noncancerous liver-infiltrating mononuclear inflammatory cells, relative to subpopulations of leukocytes, and explored how they may be relevant to leukocyte subpopulations, using the database of the human immune cell transcriptome in the Gene Expression Omnibus[3] (Geo accession no. GDS1775), which covers 26 immune regulatory cells, such as T cells, B cells, natural killer cells, macrophages, dendritic cells, basophils, and eosinophils. Among the 206 extracted, up-regulated genes in HCC-infiltrating mononuclear inflammatory cells (at the $P < 0.01$ level), 97 annotated genes were used for one-way hierarchical clusters (Fig. 1B). Most genes among 97 annotated up-regulated genes in HCC-infiltrating mononuclear inflammatory cells were shown to be expressed with higher magnitude in lipopolysaccharide-stimulated or lipopolysaccharide-unstimulated macrophages than in other types of major leukocytes. The next subpopulations, including the second most number of genes for relatively high magnitude of expression, were Th1 and Th2 CD4 cells under conditions supplemented with interleukin-12 (IL-12) and IL-4, respectively (Geo accession no.[3] GSM90858), secreting Th1 and Th2 cytokine profiles, respectively, suggesting that featured genes expressed in HCC-infiltrating mononuclear inflammatory cells were indicative of CD4 helper T cells, secreting a variety of cytokines.

Thus, this expression analysis showed that, in HCC lesions with tumor antigens, there was an accumulation of antigen-presenting cells, monocyte/macrophages, and CD4 helper T cells, which were in a cytokine-secreting condition, with enhanced cellular biological activities, including ubiquitin-proteasomal proteolysis, presumably under a hypoxic and oxidative stress environment caused by the HCC. The overall inflammatory status represented by HCC-infiltrating mononuclear inflammatory cells was not determined in terms of an anticancer effect, because no obvious shift of CD4 helper T cells to the Th1 or Th2 condition was indicated.

Distinct gene expression profile of PBMCs obtained from patients with cirrhotic liver disease complicated with HCC. The HCC-infiltrating mononuclear inflammatory cells were distinct in terms of expressed genes. The putative biological processes involving these up-regulated genes in tumor-infiltrating mononuclear inflammatory cells suggested a general influence of the HCC on the local environment of the host, represented by stress-response genes. We, thus, examined whether PBMCs in the systemic circulation of the patient might also be influenced by the development of HCC. PBMCs were obtained from 30 patients with LC associated with HCC and from 32 patients with LC not associated with HCC, and the gene expression profiles were compared (Geo accession no.[3] GSE10459).

Unsupervised hierarchical clustering analysis using 17,903 filtered genes, the expression values of which were not missing in >50% of the cases, identified two major clusters of patients, with and without HCC (data not shown). To examine the reproducibility and the reliability of the clustering, we excluded

Table 1. Biological processes for genes up-regulated in HCC-infiltrating mononuclear inflammatory cells

Biological process	−log(*P*)	Gene	ID	*t* (*T/† NT)	*P*	Cellular components‡
Antigen presentation	8.526	CD163	NM_004244	3.96	0.001	M
		CD86 antigen	NM_006889	3.28	0.006	M
		IFN, α-inducible protein 6	NM_022872	2.99	0.031	M
		IFN, γ-inducible protein 30	NM_006332	2.89	0.011	M
		Fc fragment of IgG, high affinity Ia, receptor (CD64)	NM_000566	2.85	0.013	M
		C-type lectin domain family 4, member M	NM_014257	2.73	0.020	
		CD63	NM_001780	2.51	0.024	M
		CD1D antigen	NM_001766	2.19	0.049	
Ubiqutin-proteasomeal proteolysis	6.555	Nucleoporin 107 kDa	NM_020401	4.32	0.001	
		Proteasome subunit, β type, 5	NM_002797	3.80	0.002	T, M
		Ubiquitin-conjugating enzyme E2R 2	NM_017811	3.67	0.004	
		Proteasome subunit, α type, 5	NM_002790	3.64	0.003	
		Prostaglandin E synthase 3	NM_006601	3.53	0.003	
		Ubiquitin-conjugating enzyme E2 binding protein, 1	NM_005744	2.94	0.011	
		Ubiquitin-conjugating enzyme E2E 3	NM_006357	2.75	0.017	
		DnaJ (Hsp40) homologue, subfamily A, member 1	NM_001539	2.47	0.028	
		Syntaxin 5	BC012137	2.19	0.046	
ER and cytoplasm	5.704	Chaperonin containing TCP1, subunit 8 (θ)	NM_006585	3.71	0.002	T, M
		Peptidylprolyl isomerase A	NM_021130	3.69	0.002	
		ERO1-like	NM_014584	3.03	0.009	T, M
		Peptidylprolyl isomerase C	BC002678	2.68	0.017	M
		SEC63 homologue	AF119883	2.59	0.020	
		Peptidylprolyl isomerase B	NM_000942	2.54	0.023	
		Chaperonin containing TCP1, subunit 4 (δ)	NM_006430	2.53	0.023	
		FK506 binding protein 3, 25 kDa	NM_002013	2.46	0.026	T, M
		Heat shock 70 kDa protein 5	AF188611	2.45	0.027	
mRNA processing	5.143	Small nuclear ribonucleoprotein polypeptide B	NM_003092	4.65	0.000	
		Small nuclear ribonucleoprotein polypeptide F	BC002505	3.28	0.005	T
		DEAD (Asp-Glu-Ala-Asp) box polypeptide 20	NM_007204	3.22	0.006	
		Cleavage and polyadenylation specific factor 6	NM_007007	3.16	0.010	
		Cleavage stimulation factor subunit 2	NM_001325	3.10	0.008	T
		Heterogeneous nuclear ribonucleoprotein A2/B1	NM_031243	2.94	0.010	
		PRP4 pre-mRNA processing factor 4 homologue B	NM_003913	2.90	0.020	
		Gem-associated protein 4	NM_015721	2.64	0.019	T
		LSM6 homologue	NM_007080	2.63	0.019	
		Exportin 1	NM_003400	2.42	0.029	
		RNA-binding motif protein 8A	AF127761	2.41	0.030	
		Splicing factor, arginine/serine-rich 1	M72709	2.39	0.036	
Transcription by RNA polymerase II	4.298	TAF9 RNA polymerase II	NM_016283	5.01	0.001	
		General transcription factor IIH, polypeptide 3, 34 kDa	NM_001516	4.74	0.001	
		TAF6-like RNA polymerase II	NM_006473	3.91	0.002	
		Nuclear receptor corepressor 1	AF044209	3.64	0.007	
		TATA box binding protein	NM_003194	2.89	0.018	

(*Continued on the following page*)

Table 1. Biological processes for genes up-regulated in HCC-infiltrating mononuclear inflammatory cells (Cont'd)

Biological process	−log(*P*)	Gene	ID	*t* (*T/† NT)	*P*	Cellular components‡
		Cofactor required for Sp1 transcriptional activation	NM_004270	2.82	0.014	T, M
		SUB1 homologue	NM_006713	2.59	0.021	
		General transcription factor II, I	NM_033001	2.55	0.023	T, M
		GCN5-like 2	NM_021078	2.34	0.048	
		TBP-like 1	NM_004865	2.24	0.043	
Double-strand breaks repair	3.289	RAD51 homologue C	NM_058216	5.24	0.000	T
		Werner syndrome	AF091214	4.99	0.000	T
		NIMA-related kinase 1	AK027580	3.27	0.007	
		Protein phosphatase 2	AF086924	3.24	0.023	
		Protein phosphatase 6	NM_002721	3.13	0.007	
		Proliferating cell nuclear antigen	NM_002592	2.80	0.014	T
		Topoisomerase II α-4	AF285159	2.57	0.033	T
ESR1-nuclear pathway	2.886	Nuclear receptor corepressor 1	AF044209	3.64	0.007	
		Nuclear receptor coactivator 4	X77548	3.19	0.007	
		Dopachrome tautomerase	NM_001922	3.04	0.019	
		COP9, subunit 5	NM_006837	2.77	0.014	
		Tissue specific extinguisher 1	NM_002734	2.70	0.018	M
		SCAN domain containing 1	NM_033630	2.50	0.026	
		Kinase insert domain receptor	NM_002253	2.35	0.047	
Cell cycle	2.241	Cyclin-dependent kinase inhibitor 3	NM_005192	4.60	0.000	
		Erythrocyte membrane protein band 4.1	NM_004437	3.47	0.014	
		RAN, member RAS oncogene family	NM_006325	3.38	0.004	T
		Cyclin C	NM_005190	3.14	0.008	
		Cell division cycle 42	NM_044472	3.14	0.007	
		Cyclin-dependent kinase-like 1	NM_004196	2.77	0.033	
		Cell division cycle 73	NM_024529	2.72	0.043	M
		Cell division cycle 27	NM_001256	2.57	0.043	
		Microtubule-actin cross-linking factor 1	AK023285	2.57	0.025	
		Histone cluster 1	NM_005323	2.30	0.047	
		Cyclin-dependent kinase 7	NM_001799	2.13	0.050	
		Cyclin G_2	NM_004354	2.48	0.038	
Response to hypoxia and oxidative stress	1.401	Thioredoxin	NM_003329	2.64	0.019	T, M
		Glutaredoxin 2	NM_016066	2.63	0.024	T, M
		Peroxiredoxin 3	NM_006793	2.81	0.016	T, M
		Peroxiredoxin 2	NM_005809	2.27	0.039	
		Antioxidant protein 2	NM_004905	2.22	0.042	
		Peroxiredoxin 1	NM_002574	2.21	0.043	T, M
		Microsomal glutathione *S*-transferase 2	NM_002413	2.41	0.031	M

*T represents tumor-infiltrating mononuclear inflammatory cells.
†NT represents non-tumor-infiltrating mononuclear inflammatory cells.
‡Cellular components predominantly expressed cellular components among 26 immune regulatory cells (T, Th cells; M, macrophage).

unchanged genes in all samples (genes with less than a 1.8-fold difference in >85% of samples) to remove noise. This hierarchical clustering analysis using 1,917 filtered genes confirmed two clear clusters in patients with or without HCC (Fig. 2*A*). In one major cluster, including the most LC cases, there was a subcluster, LC/HCC, which included more of the HCC patients located next to the cluster of patients with HCC (LC/HCC; Fig. 2*A*). The reproducibility of the clustering (proportion, averaged over replications and over all pairs of samples in the same cluster, BRB-ArrayTools) was 93%. Sensitivity and specificity to HCC in this cluster analysis is 88% and 76%, respectively. These cirrhotic patients without HCC were followed for at least a further 12 months to detect HCC; none of those in the LC group developed HCC over this time. The principal component analysis was performed with the filtered 1,917 genes and the two major groups; classifying LC and HCC were similarly observed (Fig. 2*B*).

To further confirm that gene expression in the PBMCs of patients with HCC was distinct from that in patients without HCC, analysis of PBMC gene expression was performed by a

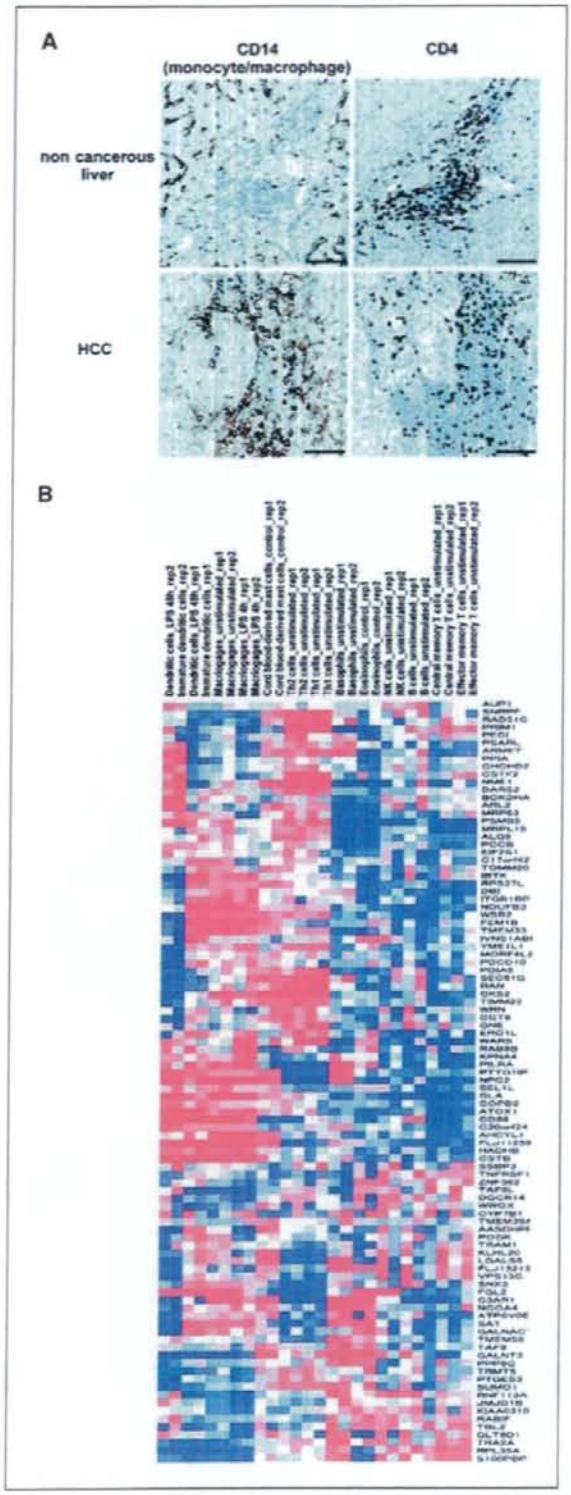

supervised learning method using categories of LC-C or HCC, age, gender, serum alanine aminotransferase (ALT), and α-fetoprotein (AFP). It showed that patients with or without HCC were significant classifiers ($P < 0.0005$), assigned with 1,430 predictor genes ($P < 0.002$; Table 2). Of 32 patients with LC, eight (25%) were misclassified as having HCC, and 2 of 30 patients with HCC (6.7%) were misclassified as not having HCC, indicating that the overall accuracy of the prediction of a patient with or without HCC was 84% (Table 2). Other clinical variables supposed to be related to HCC occurrence, such as age (ref. 29; >68 or ≤ 68 years old), gender (30), and ALT(ref. 31; >50 or ≤50 IU/L), could not differentiate gene expression in PBMCs. AFP (>20 or ≤20 ng/mL) was actually significant but was a much less powerful classifier ($P < 0.02$, assigned with 301 classifier genes). The prediction accuracy for categories of LC-C versus HCC and the AFP value >20 versus ≤20 ng/mL is not significantly affected whenever the number of predictor genes is reduced to below 62 (Supplementary Fig. S2). Taken together, these results by unsupervised and supervised analysis methods indicate that HCC development in LC-C patients significantly affects the gene expression profile in PBMCs.

Features of biological processes for which gene expression was significantly altered in PBMCs in HCC patients. We next examined the biological processes possibly affected by HCC development, given the expression profiles in PBMCs from patients with HCC. Statistical analysis showed that 867 genes were up-regulated and 989 genes were down-regulated in PBMCs from patients with HCC, compared with those without HCC ($P < 0.005$). Six representative genes, *Ccr1*, *Hat*, *Map2k1ip1*, *PigB*, *Tlr2*, and *Sod2*, were randomly selected from genes which were biologically important and differentially expressed between LC and HCC groups, and their expression was confirmed by RTD-PCR (Supplementary Fig. S3*A*). To exclude the possibility of circulating cancer cells, we have also examined the expression of *Afp*, *Krt8*, *Krt18*, and *Krt19*. No expression was detected for *Afp* (data not shown), and no statistically significant difference was found for expression of *Krt8*, *Krt18*, and *Krt19* between patients with HCC and without HCC (Supplementary Fig. S3*A*). The expression data were also confirmed by flow cytometric analysis. We evaluated how many cells in blood expressed CCR1 and CCR2 and confirmed that populations expressing CCR1 and CCR2 were significantly higher in PBMCs from patients with HCC than those without (Supplementary Fig. S3*B*). To understand the biological processes in PBMCs for which up-regulated or

Figure 1. HCC-infiltrating mononuclear inflammatory cells involve monocyte/macrophage and helper T cell. *A*, immunohistochemical staining. Many of the HCC-infiltrating mononuclear inflammatory cells expressed monocyte/macrophage marker, CD14. In contrast, few CD14-positive cells were seen in noncancerous liver-infiltrating mononuclear inflammatory cells. *Bars*, 100 μm. *B*, one-way hierarchical clustering analysis of gene expression of immune-mediating cells with genes whose expression was up-regulated in HCC-infiltrating mononuclear inflammatory cells. Data for gene expression in immune-mediating cells were retrieved from Gene Expression Omnibus[2] (Geo accession no. GDS 1775). By excluding genes missing from over half of the immune-mediating cells, 206 genes up-regulated in HCC-infiltrating mononuclear inflammatory cells were filtered, and the remaining 97 genes were used for clustering. Transverse and longitudinal titles show the type of immune-mediating cell and gene symbols, respectively. Color indicates relative expression magnitude of 97 up-regulated genes HCC-infiltrating mononuclear inflammatory cells among retrieved expression data of major leukocyte types deposited in the public database. The red and blue color means relatively high or low magnitude of expression among 26 retrieved expression data of leukocytes. The heat-map shows that helper T cells and unstimulated or stimulated macrophages included more blocks with the red color.